Dynamics of Colloids in Single Solid-State Nanopores

ARTICLE *in* THE JOURNAL OF PHYSICAL CHEMISTRY B · MARCH 2011

Impact Factor: 3.3 · DOI: 10.1021/jp200326w · Source: PubMed

8 AUTHORS, INCLUDING:

Laurent Bacri
Université d'Évry-Val-d'Essonne
35 PUBLICATIONS **573** CITATIONS
SEE PROFILE

Abdelghani Oukhaled
Université de Cergy-Pontoise
28 PUBLICATIONS **617** CITATIONS
SEE PROFILE

Gilles Patriarche
French National Centre for Scientific Research
545 PUBLICATIONS **6,334** CITATIONS
SEE PROFILE

Loïc Auvray
Paris Diderot University
132 PUBLICATIONS **3,021** CITATIONS
SEE PROFILE

THE JOURNAL OF PHYSICAL CHEMISTRY B

ARTICLE

pubs.acs.org/JPCB

Dynamics of Colloids in Single Solid-State Nanopores

L. Bacri,*[,†] A. G. Oukhaled,[†,‡] B. Schiedt,[†,‡] G. Patriarche,[‡] E. Bourhis,[‡] J. Gierak,[‡] J. Pelta,[†] and L. Auvray[§]

[†]LAMBE UMR CNRS 8587, Evry and Cergy-Pontoise University, France

[‡]LPN/CNRS, UPR 20, Marcoussis, France

[§]Matière et Systèmes Complexes, UMR 7057, Paris Diderot University, France

ABSTRACT:

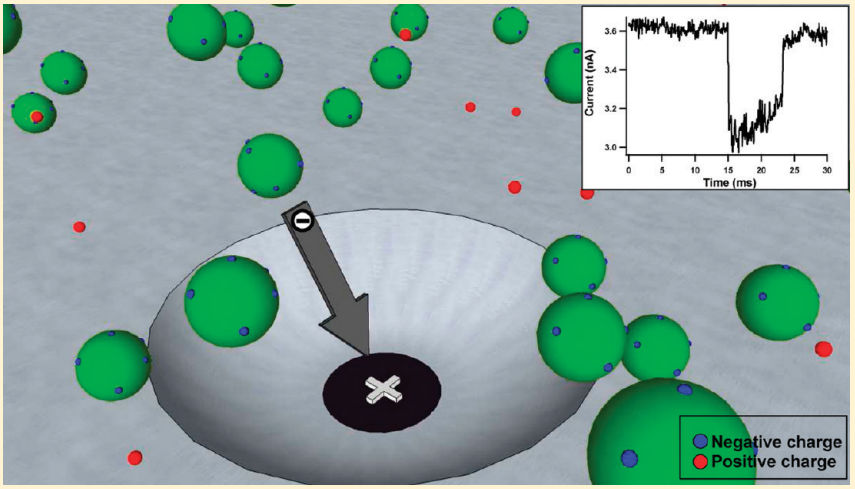

We use solid-state nanopores to study the dynamics of single electrically charged colloids through nanopores as a function of applied voltage. We show that the presence of a single colloid inside of the pore changes the pore resistance, in agreement with theory. The normalized ionic current blockade increases with the applied voltage and remains constant when the electrical force increases even more. We observe short and long events of current blockades. Their durations are associated, respectively, with low and high current variation. The ratio of long events increases with the electrical force. The events frequency increases exponentially as a function of applied voltage and saturates at high voltage. The dwelling time decreases exponentially at low and medium voltages when the electrical force increases. At large voltages, this time decreases inversely proportionally to the applied voltage. The long events are associated with translocation events. We show that the dynamics of colloids through the nanopore is governed mainly by two mechanisms, by the free-energy barrier at relatively low and medium voltages and by the electrophoresis mechanism at high voltage.

INTRODUCTION

Fifty-seven years ago, W. H. Coulter invented a device allowing one to analyze the size and concentration of particles dispersed in a solution.[1] This device consists of a measurement of electrical resistance variation of a 10 μm hole that connects two electrolyte-filled chambers. By applying either an electrical field or a hydrodynamic drag, the particle passes from one chamber to the other through the hole. The presence of a particle inside of the hole generates a sharp increase of the hole resistance associated with an abrupt current blockade. The magnitude of this current blockade is proportional to the size of the particle. The number of current blockades is related to the particle concentration, and the width of the current blockade is due to the dynamics of the object within the pore. This device was used to measure the size of microscale analytes[2] such as biological cells. To improve the sensitivity of the device to detect colloidal[3] or biological objects of diameter higher than 60 nm, such as viral particles,[4] R. W. Deblois and C. P. Bean reduced the diameters of the holes to about 300−500 nm in porous polycarbonate membranes produced by the track-etching technique. These pores were of cylindrical shape with a length of about 3 μm. The authors showed that they could determine the particle concentration, the electrophoretic velocity of the particles, and the electroosmotic velocity of the fluid in the pore (330 nm diameter) in the case of 109 nm latex spheres. Moreover, they observed the difference between bacteriophages (T2 and T4) with full and empty capsids of DNA. Following this idea, S. M. Bezrukov incorporated alamethicin ion channels in lipid membranes and has shown for the first time that these channels could be used as molecular Coulter counters[5] at the nanometer scale below the 60 nm lower limit of the classical Coulter counter techniques.

Received: January 12, 2011
Revised: February 18, 2011
Published: March 10, 2011

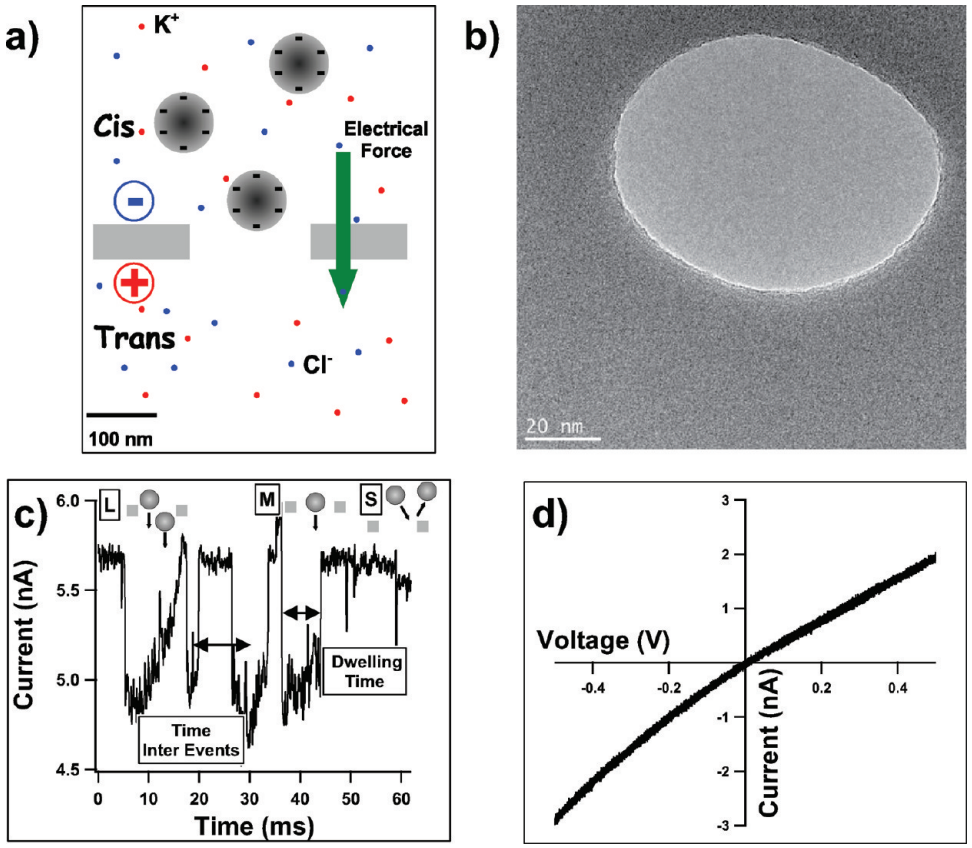

Figure 1. Solid-state nanopore for sensing individual nanoparticles. (a) Schematic diagram of the experimental setup, consisting of a 175 nm pore drilled by a fast ion beam (FIB) in an ultrathin Si_3N_4 membrane. A difference of voltage is applied across the membrane by two electrodes inserted into each reservoir filled by an electrolyte (KCl 10 mM). Silica particles are driven by a high electrical field into the pore. (b) A transmission electron microscopy (TEM) image of one nanopore drilled by a FIB. The nanopore size is 68 × 88 nm. (c) Typical current trace showing the dwelling of 85 nm silica particles through the nanopore. The applied voltage is 900 mV. Each event is characterized by the corresponding dwelling time T_t. Moreover, we measure the inter-events time in order to calculate the characteristic events frequency (cf. Figure 4a). The schematic insets illustrate colloids inside of the pore which bump against the entrance of the pore (S) or cross alone (M) or are followed by a second colloid (L) through the pore. (d) Current−voltage ($I-V$) curve of a solid-state nanopore in 10 mM KCl. The rectification, characterized by a slightly nonlinear $I-V$ curve, is due to the shape of the nanopore.

Several groups have since used protein channels as sensor for small molecules or macromolecules, including neutral polymers,[6,7] charged polymers,[8−11] DNA,[12−14] and, more recently, proteins.[15,16]

Toxin channels have good sensing capabilities for probing macromolecules because their diameter is comparable to the molecule size. On the other hand, proteins channels are sensitive to aggressive environments like temperature, pH, salt concentration, and denaturing agents.[17]

One way of enlarging the applicability of protein channels as Coulter counters and getting around limitations in their use, such as the fragility of lipid membranes and the lack of variability in the pore sizes, was to fabricate stable artificial nanopores. Different strategies have been used to perform nanometer-scale devices, including PDMS channels for sensing polydisperse colloidal solutions and molecules,[18−20] multiwalled carbon nanotubes for studying mass transport using polystyrene spheres as probes,[21] solid-state nanopores,[22,23] single channels having a conical shape,[24] and glass pipettes[25,26] for sensing biomolecules.

Single carbon nanotubes have already been used as Coulter counters to measure the diameter and electrophoretic mobility of negatively charged polystyrene nanoparticle in confined media.[21,27−29] Demonstration of transport of three different polystyrene nanoparticle sizes through cylindrical nanopores of 360 nm lengths with diameters in the range of 78−240 nm fabricated using standard silicon processing techniques was reported recently by Petrossian et al.[30] These few experiments show many applications of the Coulter counter principle to molecule transport measurements.

Up to now, the dynamics of colloid transport through solid-state nanopores as a function of applied voltage has not been probed. To get a better insight into these effects, we investigate a regime where the pore diameter (140 × 175 nm) is larger than the pore length (50 nm) and larger than the particles (85 nm). The entry of a colloid in the nanopore causes a decrease in the single nanopore ionic current. We analyze and discuss these pore resistance changes by the presence of single colloids within the pore, the frequency of current blockades, the normalized blockade current, the number of translocation events, and the dwelling time as a function of applied electrical driven force. Current blockades were characterized by three types of mean blockade times, short ones associated to low current blockade levels and medium and long ones with high current blockade levels. The normalized current blockade and the ratio of long events increase

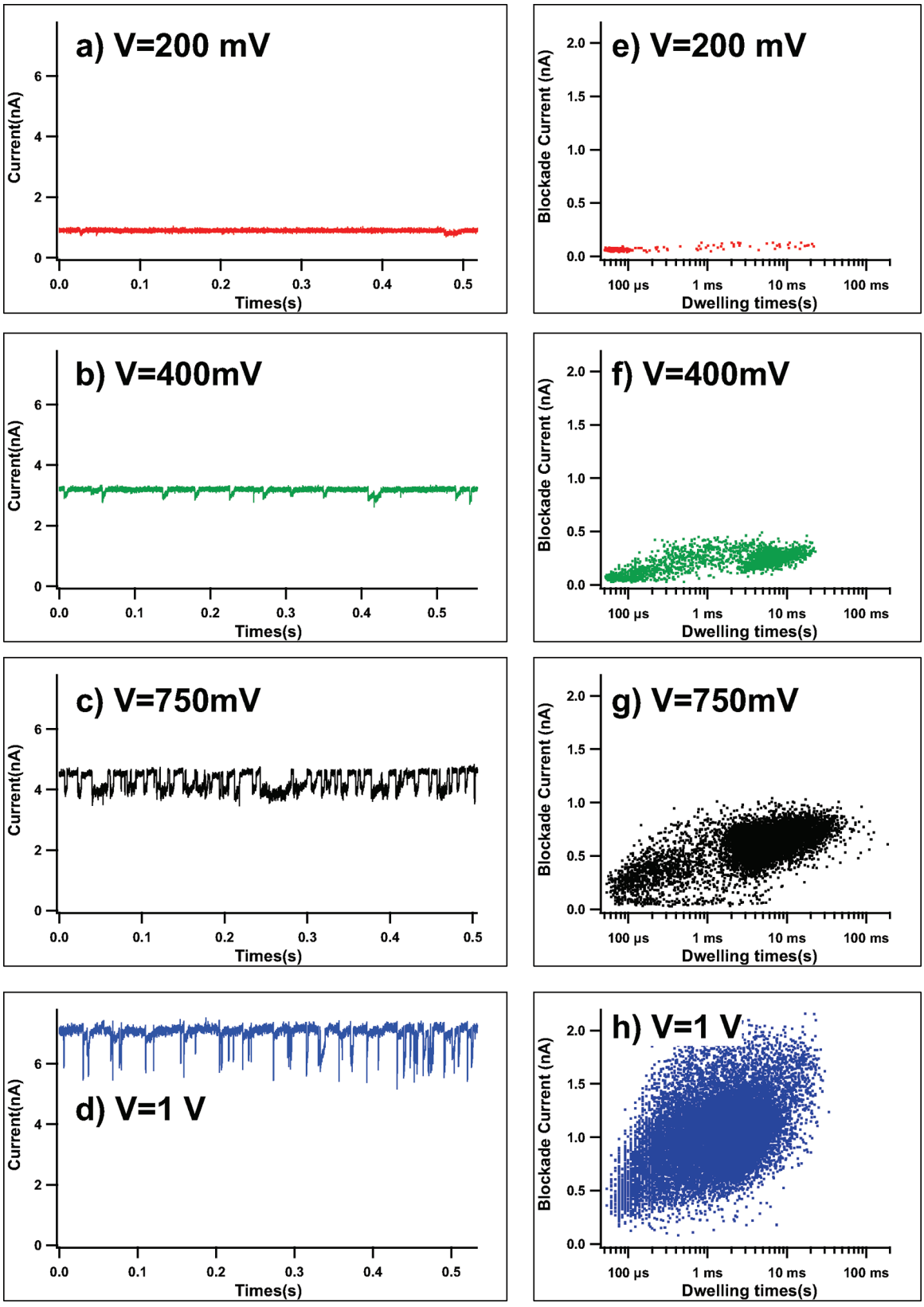

Figure 2. Current−time traces of 85 nm silica particles through a 175 nm pore diameter recorded at different applied voltages (a−d) and their respective event scatter plot of dwelling time versus blockade current (e−h). The event rate becomes larger as the applied voltage is increased; however, the dwelling time becomes shorter as the applied voltage is increased.

dx.doi.org/10.1021/jp200326w |*J. Phys. Chem. B* 2011, 115, 2890–2898

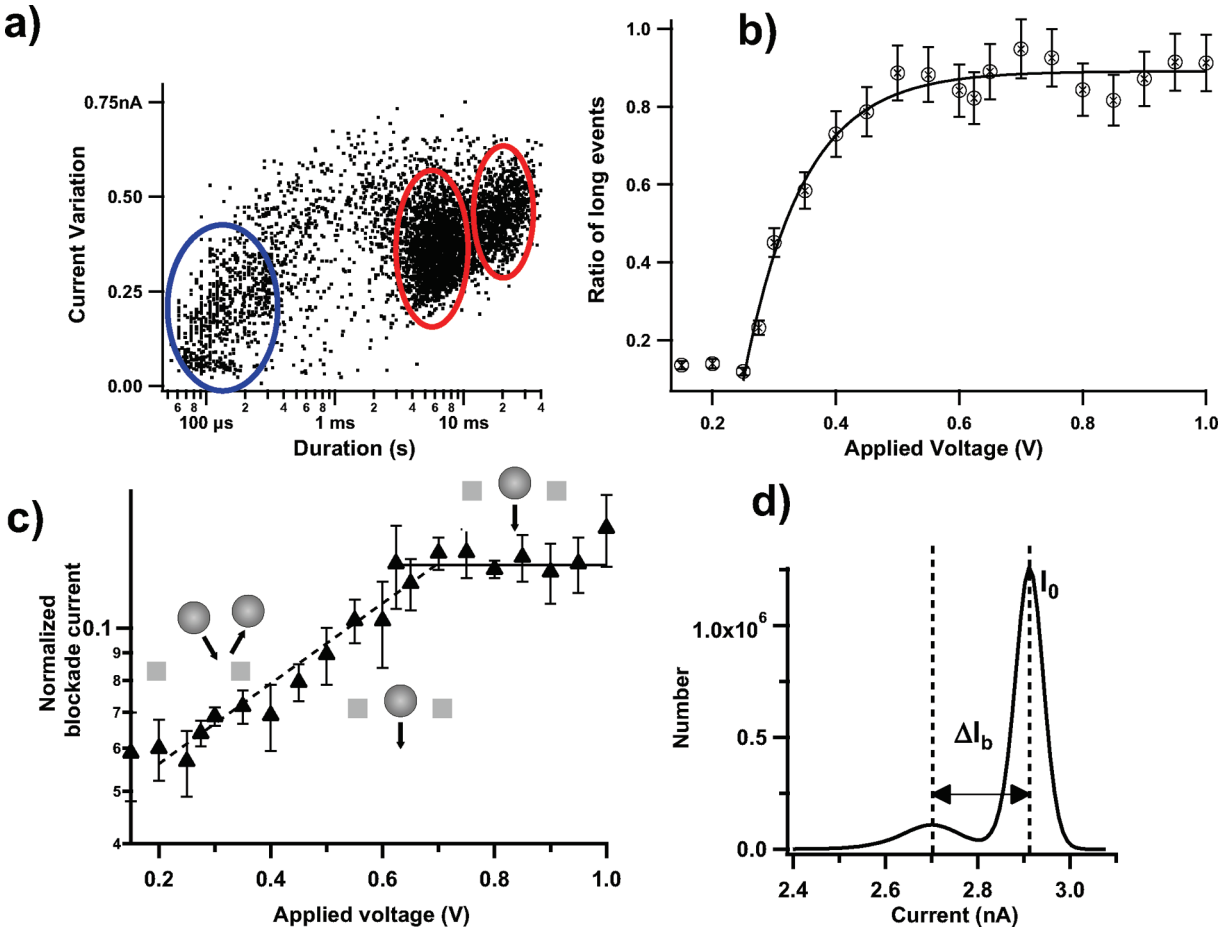

Figure 3. (a) Event scatter plot of dwelling time versus blockade current used to count each short (type S), medium (type M), or long (type L) event when $\Delta V = 500$ mV. (b) Ratio $r = N_{long}/(N_{long} + N_{short})$ between the numbers of long (N_{long}) (type M and L events) and short (N_{short}) type S events as a function of the applied voltage V. The fit curve is an exponential function $r_{final} - A\exp(-V/V_0)$, where $r_{final} = 0.9 \pm 0.02$, $A = 0.78 \pm 0.02$, and $V_0 = 110 \pm 10$ mV. (c) Normalized blockade current $\Delta I_b/I_0$ as a function of the applied voltage. The fit curve is an exponential function $A_1\exp(V/V_1)$, where $A_1 = 0.05 \pm 0.002$ and $V_1 = 586 \pm 52$ mV. (d) Histogram of the ionic current when $\Delta V = 500$ mV. I_0 is the base current and ΔI_b the blockade current.

when the applied voltage increases and remain constant at high voltage. The short events are associated with interactions between the colloids and the entry of the nanopore. The long events could be associated with a translocation time or a dwelling time. The mean long time decreases exponentially at relatively low applied voltage and linearly at high voltage. This result shows that the dynamics of colloids through the nanopore is governed mainly by two mechanisms, by a free-energy barrier at relatively low voltage (most probably due to electrostatic interactions) and by an electrophoresis mechanism at high voltage.

MATERIALS AND METHODS

The experimental setup is shown in Figure 1a, depicting a silica nanoparticle that is captured and passes through the nanopore from the cis side to the trans side due to an applied electrical field. The particles are present only in the cis side. A nanoparticle passing through the pore causes a transient in the measured electrical current, as shown in Figure 1c; these transient pulses can be correlated to the size, mobility, and concentration of the nanoparticles.

Solid-State Nanopore. The nanopores are drilled into DuraSiN chips (3×3 mm^2, Protochips Inc., U.S.A.) featuring a 50 nm thick silicon nitride membrane (50×50 μm^2). The nanopore sizes are 140×175 nm. The nanopore is obtained by a highly focused ion beam (FIB). The FIB allows the drilling of each hole in one step. In a whole membrane, the ion dose is calibrated to obtain always the same size for each hole. Calibration of the ion dose needed to create a certain pore diameter is done on a spare membrane coming from the same wafer. Depending on the ion dose, we can obtain a great variety of nanopore sizes from 4 to 5 nm[31] to several hundred nanometers (cf. Figure 1b). In this work, we have chosen a size of 160 nm in order to observe the large objects, such as the colloids.

In order to increase the hydrophilicity of nanopores, membranes have been either subjected to an oxygen plasma for 3 min for each side or plunged into a Piranha solution (30 vol % H_2O_2/H_2SO_4 1:1) for 30 min. Then, each membrane containing one nanopore is mounted with a fast-curing two-component silicone glue (KwickCast, Word Precision Instruments, Inc.) onto a plastic screw cap having a hole of 1.8 mm. This cap is specially designed to be used by the planar patch clamp device "Port-a-patch" (Nanion Technologies GmbH).[31] This high-performance and flexible instrument is the base of our experimental setup. It consists of a shielded Axon 200B headstage. Its output is connected to a first Ag/AgCl electrode.

dx.doi.org/10.1021/jp200326w |J. Phys. Chem. B 2011, 115, 2890–2898

Drops of electrolyte are put on each side of the membrane, and a second Ag/AgCl electrode closes the circuit.

Colloids. The colloids have been synthetized by the Stoeber method.[32] These silica nanoparticles (SiO_2) are negatively charged. They are characterized by light scattering and TEM;[33] the size distribution is monodisperse with a diameter of 85 nm. The particles are dispersed in ionic 10 mM KCl solution.

Data Acquisition. Data are filtered at 10 kHz and acquired at 4 μs intervals with the Digidata 1440A digitizer coupled with Clampex software (Molecular Device, Union City, CA). Each event is detected with the data treatment software Igor Pro (WaveMetrics Inc.). The measurements are based on statistical analysis of the characterization of all events. Events translocation was observed in only a very small percentage of our fabricated nanopores.

RESULTS AND DISCUSSIONS

Behavior of the Current Blockade As a Function of Applied Voltage. In the presence of colloids, we observe current blockades (Figure 2). When the applied voltage increases, the mean current baseline and the number of current blockades increase too. We characterize the recorded events by their dwelling time and current blockade, as shown in Figure 2e−h. At low voltage ($\Delta V \leq 250$ mV), the events are very rare, and their blockade levels are very small. However, many event blockades are observed at higher applied voltages ($250 \leq \Delta V \leq 1000$ mV). The events can be well classified in two groups, short events with durations of a couple of tens of microseconds and a low current blockade (type S events in Figure 1c). These peaks are explained by bumping events at the entrance of the pore.[10] Other types of events are characterized by longer duration than the short events and a higher current blockade (type M medium events and type L long events). The type M events last a couple of milliseconds. The type L events are 20 ms long (cf. Figures 1c and 3a).

By increasing the applied voltage, the population of long events shifts toward the population of short events (Figure 2f, g) and becomes indiscernible from them at very high voltage (Figure 2h). At all voltages, the current blockade of long events is larger than that of short events.

Indirect Evidence of Colloids Translocation. Figure 3a is the plot of the current variation of each event versus its duration when the applied voltage is $\Delta V = 500$ mV. We observe three clouds, the first one related to the type S short events with a mean time of around 200 μs, the second one related to the type M medium events with a mean duration of around 7 ms, and the third one related to the type L long events around 20 ms.

We analyze our data in detail; Figure 3b describes the proportion of long events, defined as the ratio of types M and L together to all events as a function of applied voltage. This ratio increases exponentially as the applied voltage increases. From the exponential fit $\exp(-V/V_c)$, we calculate a characteristic voltage $V_c = 95 \pm 10$ mV. This fitted value is close to the minimal applied voltage, $\Delta V = 150$ mV, allowing experimentally the observation of current blockades. At voltages higher than 600 mV, the proportion of long events does not further increase but reaches a steady value at 89 ± 2%. This suggests the existence of a potential barrier around 600 mV to allow the particle transport through the solid-state nanopore. Beyond 600 mV, the observed events are mainly long and are consistent with the translocation of silica particles. The remaining population (type S events) corresponds to silica interacting with the pore but failing to cross the pore.

Figure 3c shows the normalized blockade current $\Delta I_b/I_0$ as a function of the applied voltage ΔV. We observe two regimes in the curve. When the applied voltage is below 600 mV, the normalized blockade current increases exponentially with the applied potential. This increasing behavior could be explained by the method used to estimate ΔI_b and I_0. The current histogram of Figure 3d allows the forecast of ΔI_b and I_0. The first Gaussian peak describes both short (type S) and long (type M + L) blockades. The position of its maximum is related to an average between bumping and dwelling events. As the ratio between the two types of events increases exponentially with the voltage (cf. Figure 3b), the normalized blockade current varies exponentially in the same manner. We suppose that the electrical forces allowing the colloids to translocate massively through the pore are too weak in this voltage regime. When the voltage is bigger than 600 mV, we observe that the ratio $\Delta I_b/I_0$ reaches a plateau of value 0.13 ± 0.002. In this second regime, the nanoparticles are blocking the pore similarly whatever the applied potential, showing that the particle passes through the pore. In this regime, the ratio of long events reaches its upper value.

Analysis of the Pore Resistance in the Absence and Presence of Colloids. It is interesting to estimate the resistance variation caused by the presence of one particle inside of the pore. Let us consider a cylindrical pore of diameter D drilled in an insulating dielectric membrane of length L separating two electrolyte-filled compartments of electrical conductivity σ. A voltage is applied between the cis and trans compartments.

The electrical resistance R of the empty pore in the first approximation is given by[34] $R_1 = (1/\sigma)\int_{z=-L/2}^{L/2}(dz/A(z))$, where $A(z) = (\pi D^2/4)$ is the cross sectional of the empty pore, $R_1 = (4L/\sigma\pi D^2)$.

The presence of single colloids inside of the pore increases the pore resistance, as was previously described.[3,19] Our experimental setup is similar to Saleh's setup.[19] In both cases, the pore diameter is about 100−200 nm, but in our study, the pore length is very thin, 50 nm, compared with that of Saleh's pore (3 μm).

To calculate the maximal pore resistance R_2 caused by the colloids, first we consider the colloids in the middle of the pore, and then, we calculate the free area $A_2(z)$ between the colloids and the pore wall, $A_2(z) = A(z) - A_1(z)$, where $A_1(z) = \pi((d^2/4) - z^2)$ is the cross section of colloids of diameter d; then, we obtain

$$A_2(z) = \frac{\pi}{4}(D^2 - d^2)\left[1 + \frac{4z^2}{D^2 - d^2}\right]$$

The pore resistance is given by

$$R_2 = \frac{1}{\sigma}\int_{z=-L/2}^{L/2}\frac{dz}{A_2(z)} = \frac{4}{\sigma\pi(D^2 - d^2)}\int_{-L/2}^{L/2}\frac{dz}{1 + \frac{4z^2}{D^2 - d^2}}$$

and by integration by substitution ($\tan\varphi = (2z/(D^2 - d^2)^{1/2})$), we obtain

$$R_2 = \frac{4}{\sigma\pi D}\frac{1}{\sqrt{1 - \left(\frac{d}{D}\right)^2}}\operatorname{atan}\left[\frac{L}{D}\frac{1}{\sqrt{1 - \left(\frac{d}{D}\right)^2}}\right]$$

and the maximal variation of the resistance is

$$\Delta R = R_2 - R_1 = \frac{4}{\sigma\pi D}\left[\frac{\mathrm{atan}\left[\frac{L}{D}\frac{1}{\sqrt{1-\left(\frac{d}{D}\right)^2}}\right]}{\sqrt{1-\left(\frac{d}{D}\right)^2}} - \frac{L}{D}\right]$$

Under our experimental conditions, we obtain $R_1 \cong 1.62 \times 10^6\ \Omega$ and $R_2 = 2.04 \times 10^6\ \Omega$, and the relative increase in resistance is given by $1 - (R_1/R_2) \cong 0.2$; this relative increase in resistance is proportional to the relative blockade current $1 - (I_b/I_o) = (\Delta I_b/I_o)$. We measure experimentally this value; $(\Delta I_b/I_o)$ reaches a steady value 0.13 ± 0.002, as was described above (cf. Figure 3c). The estimations yield the right order of magnitude of the observed value. The difference between both values can be explained by the fact that the colloids do not enter necessarily by the middle of the pore, as assumed in our calculations. Furthermore, in favorable cases, we observe events where their relative current blockades are very close to the theoretical value.

Events Frequency and Energy Barrier Estimation. From the events time positions (cf. Figure 1c), we measure the inter-events times. The distribution of these times is fitted with an exponential function (Figure 4a). The inverse of the characteristic time of the exponential function is the events frequency f. In Figure 4a, we calculate $f = 38.5 \pm 2$ Hz for $V = 600$ mV. This frequency increases exponentially with applied voltage (Figure 4b). When the voltages are larger than 800 mV, the frequencies reach a steady value (107 ± 1 Hz). This is simply a saturation effect; this frequency corresponds to a mean blockade duration of around 9.3 ms, and this mean blockade time is experimentally observed (Figure 5f).

The events frequency f is described by a Van't Hoff−Arrhenius law:[35] $f = f_0 \exp(V/V_0)$, where $f_0 \approx \nu \exp(-U^*/k_BT)$ is the zero-voltage events frequency governed by an activation barrier U^* (ν is a frequency factor) and $(|V|/V_0) = (zeV/k_BT)$ is a barrier reduction factor acting on ze, the effective charge of the silica particle, and due to the applied voltage V. From the exponential fit, we obtain $f_0 = 3.9 \pm 0.2$ Hz and $V_0 = 272 \pm 2$ mV, and we deduce the apparent charge number z of the colloid, $z = 0.1 \pm 0.001$. This value is really underestimated. Costa et al. have previously observed a reduction of the apparent charge number of the colloids,[36] probably due to K^+ ions interaction within the negatively charged particles.

To obtain an estimation of the activation barrier (U^*), the frequency factor (ν) is estimated by a barrier penetration calculation $\nu = CD_{diff}A_{pore}/L_{pore}$, where $C = 2.0 \times 10^{18}$ particles/m^3 is the bulk concentration of silica nanoparticles, $D_{diff} = 5 \times 10^{-12}$ m^2/s is their calculated diffusion coefficient according to the Stokes law, $A_{pore} \approx 96 \times 10^{-15}$ m^2 is the cross-sectional area of the pore, and $L_{pore} \approx 50 \times 10^{-9}$ m is the pore length. We calculate $\nu \approx 4.9$ Hz and $U^* \approx 0.24k_BT$. This activation barrier is very low. As the nanopore size (175 nm) is very large compared to the colloid size (85 nm), we suppose that the particles are not confined in the pore and do not need to overcome a high-energy barrier to enter into the pore, as is the case of random coil when the diameter of the flexible chain is larger than the pore diameter. This is observed experimentally for polyelectrolytes,[10,11] DNA,[35] unfolded proteins[15] with an α-hemolysin pore and with unfolded proteins with aerolysin channel,[37] and with unfolded proteins with solid-state nanopores.[38]

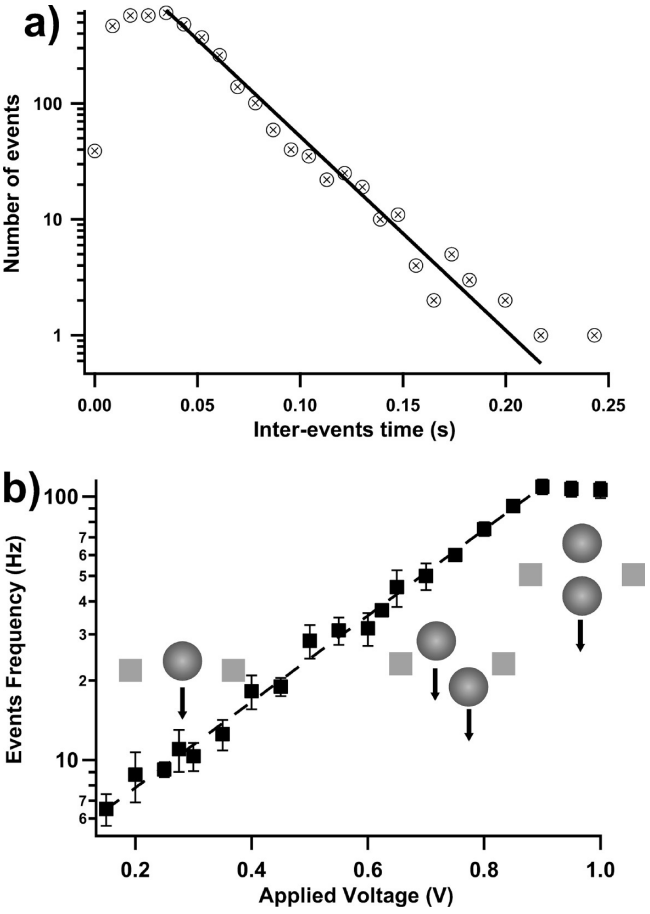

Figure 4. (a) We fit the inter-events times histogram with an exponential law (black line) in order to calculate the events frequency $f = 38.5 \pm 2$ Hz for $\Delta V = 600$ mV. (b) Events frequency as a function of the applied voltage. The dotted line is an exponential fit, $f = \exp(|V|/V_0)$, where $f_0 = 3.9 \pm 0.2$ Hz and $V_0 = 272 \pm 2$ mV.

Dwelling Times versus Applied Voltage. After the detection of each event, we measure their duration. In Figure 5a and b, we have plotted the histograms of these durations in two cases, $V = 400$ and 800 mV. The dotted lines are calculated from the integration of the histograms and represent the integrated probability[15] to observe one event of the chosen duration. Each peak corresponds to a single gap. Each gap is fitted by an exponential function $A \exp((\tau - \tau_0)/\tau_c)$, where τ_c is a characteristic time and τ_0 the position of each peak.

In the first case, we observe two peaks; the first one is linked to the collision between the particle and the nanopore (type S, $\tau_c = 60 \pm 5\ \mu$s), and the second one is linked to the dwelling times inside of the pore (type M, $\tau_c = 7.3 \pm 0.1$ ms). In the second case, we observe three peaks, the "short time" peak (type S, $\tau_c = 170 \pm 25\ \mu$s), the "medium dwelling time" peak (type M, $\tau_c = 3.4 \pm 0.2$ ms), and a "long time peak" (type L, $\tau_c = 9 \pm 0.1$ ms).

We have plotted the type M and type L dwelling times as a function of the inverse of the applied voltage (Figure 5c and e) and as a function of the applied potential (Figure 5d and f). In the

dx.doi.org/10.1021/jp200326w |J. Phys. Chem. B 2011, 115, 2890–2898

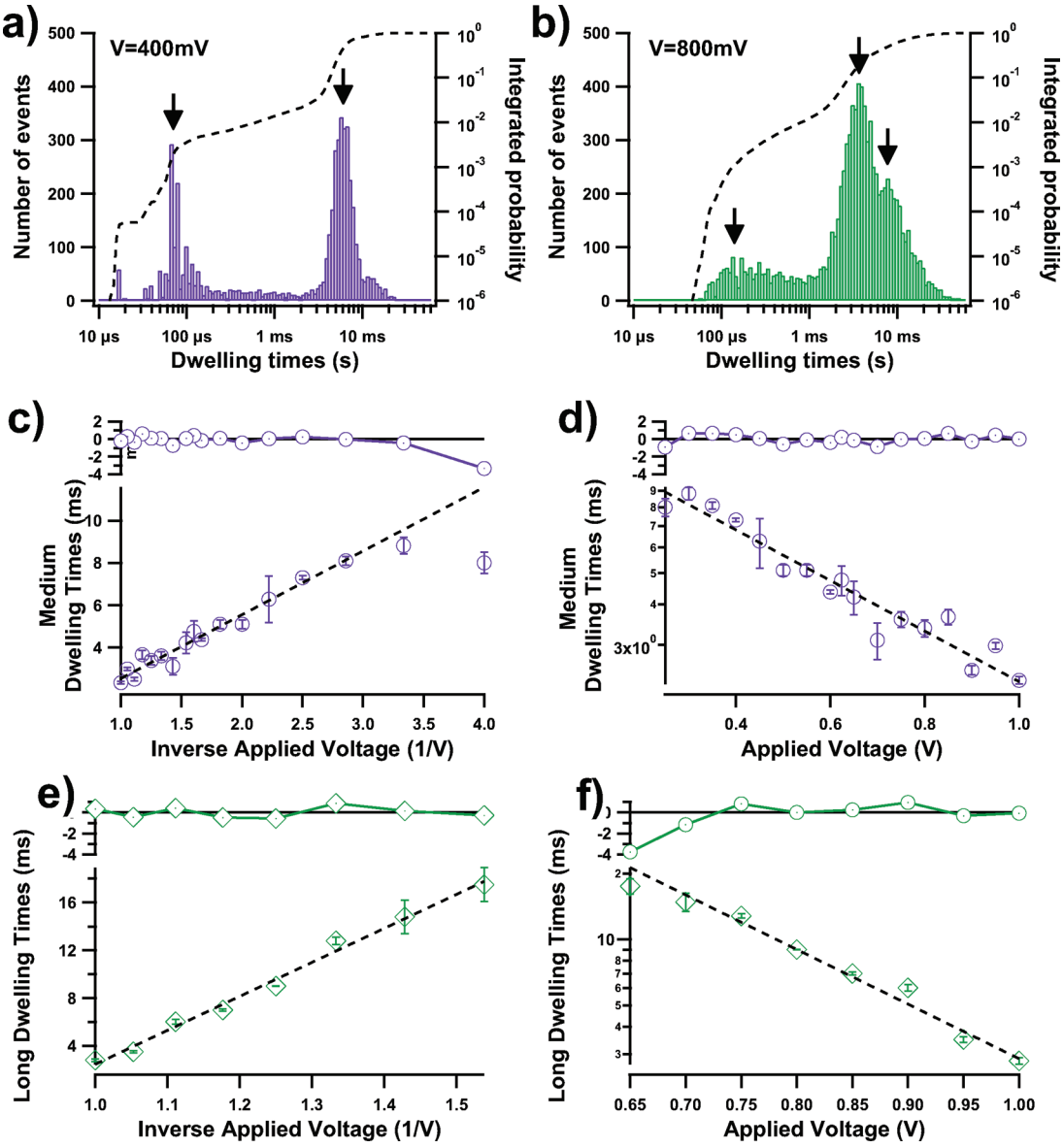

Figure 5. Voltage dependence of dwelling times. (a,b) Distributions of dwelling time, respectively, at 0.4 V with a medium characteristic dwelling time of 7.3 ± 0.1 ms and at 0.8 V with two characteristic times, medium (3.4 ± 0.2 ms) and long (9.0 ± 0.1 ms). Each dwelling time value is extracted from an exponential fit of the integrated probability curve (dotted curves). (c,e) Respectively, medium and long dwelling times as a function of inverse applied voltage. The dashed lines are linear fits of equations $a/\Delta V + b$. For the medium times, $a = 3.0 \pm 0.05$ ms·V and $b = -0.47 \pm 0.08$ ms. For the long times, $a = 29 \pm 1$ ms·V and $b = -26 \pm 1.5$ ms. (d,f) Respectively, medium and long dwelling times as a function of applied voltage. The dashed lines are exponential fits of the equation $A \exp(-\Delta V/V_c)$. For the medium times, $A = 8.9 \pm 0.3$ ms and $V_c = 554 \pm 40$ mV. For the long times, $A = 21.3 \pm 0.3$ ms and $V_c = 175 \pm 3$ mV. The upper graphs represent the deviation from the fits.

first case, we suppose that the dwelling phenomena are governed by the applied electric force $\tau_c \approx 1/V$.[39,40] In the second case, we model the dwelling times with a free-energy barrier model $\tau_c \approx \exp(-\Delta V/V_c)$.[41]

When we compare both fits of the medium times (type M), we prefer the exponential fit according to the residual curves when the applied voltage is smaller than 650 mV. From this exponential fit, we calculate a characteristic voltage $V_c = 554 \pm 40$ mV. In this model, the applied voltage must be higher than V_c so that the colloids go through the pore. Physically, the particles must overcome a free-energy barrier, called translocation energy, in order to translocate through the pore. In the ratio of long events (type M + L) curve (cf. Figure 3c), at the same applied voltage, the type M and L events become the majority (60%). After overcoming the translocation energy, the particle goes through the pore. Considering the fits of the two behaviors, we could prefer the behavior driven by the electric force for the voltages higher than 650 mV for type M events.

Indeed, for the voltages higher than 650 mV, we observe clearly a second scatter (cf. Figure 5b), characterized by type L dwelling times. In Figure 5e,f, we observe that the $1/V$ fit is more convenient. Then, we could conclude that we observe a behavior governed by the particle mobility. We could suppose that the type L times are due to the presence of a first particle at the entrance of the pore and a second one at the exit of the pore (cf. Figure 1c).

dx.doi.org/10.1021/jp200326w |J. Phys. Chem. B 2011, 115, 2890–2898

When the voltage is higher than 900 mV, we observe that the type M and type L dwelling times become similar. According to the events frequency curve, we could suppose that the colloids enter inside in single line when we observe the frequencies saturation (cf. Figure 4b).

From the frequencies curve, we have observed that the particles do not need to cross a high-energy barrier to enter inside of the pore because the colloids are large (85 nm) and the nanopore is much bigger (175 nm).

From the other curves, we have observed two main regimes. The first one below 400 mV is governed by a low-energy-barrier process. The second one above 400 mV is governed by the electric force. If this force is too high ($V > 650$ mV), we observe two behaviors, one single particle in the pore (type M) and two particles in the pore (type L). When the voltage is too high, we observe a saturation; the colloids go through the pore in a single queue.

CONCLUSION

We have demonstrated by using FIB the possibility to produce a large nanopore where the pore diameter (175 nm) is larger than the membrane thickness (50 nm). We used this pore as a Coulter counter to probe the passage of large colloids (85 nm) larger than the membrane thickness (50 nm) in order to build a model system for nanopore electrical charged particle translocation. We highlighted stochastic information about transport parameters by investigating the pore resistance changes by the presence of single colloids within the pore, the frequency of current blockades as a function of applied electrical forces, the dwelling time, and the activation energy. We show in favorable cases that the measured relative increase in pore resistance is in agreement with the predicted theoretical value. The events frequency dependency is exponential as a function of the applied electrical forces, meaning that the arrival of colloids in the pore is random and that two successive arrivals are not correlated. Furthermore, we have found that the frequency of passage saturates at very high voltage (>0.8 V) because of colloid accumulation at the entrance of the pore due to the large electric field.

The dwelling time decreases as a function of voltage. At low voltage, the time dependence is exponential, showing that the colloid transport is governed by the free-energy barrier. At high voltage, the time dependence is linear, evidence that the dynamics of colloids through the nanopore is governed by the electrophoresis mechanism. We have found a low value of the energy barrier as expected because in our configuration, the pore diameter is larger than the pore length and the colloid diameter, and in addition, the colloids size is larger than the pore lengths.

ACKNOWLEDGMENT

This work was supported by a grant, Action Thématique Incitative Génopole, ANR Blanche "TRANSFOLDPROT" BLAN08-1_339991, and by ANR "ACTIVE NANOPORES" N° ANR-06-NANO-028. We also thank Jerôme Mathé for useful discussions.

REFERENCES

(1) Coulter, W. H. U.S. Patent 2,656,598, 1953.
(2) Kubitschek, H. E. *Nature* **1958**, *182*, 234–235.
(3) Deblois, R. W.; Bean, C. P. *Rev. Sci. Instrum.* **1970**, *41*, 909–916.
(4) Deblois, R. W.; Bean, C. P.; Wesley, R. K. A. *J. Colloid Interface Sci.* **1977**, *61*, 323–335.
(5) Bezrukov, S. M.; Vodynoy, I.; Parsegian, V. A. *Nature* **1994**, *370*, 279–281.
(6) Bezrukov, S. M.; Vodyanoy, I.; Brutyan, R. A.; Kasianowicz, J. J. *Macromolecules* **1996**, *29*, 8517–8522.
(7) Movileanu, L.; Bayley, H. *Proc. Natl. Acad. Sci. U.S.A.* **2001**, *98*, 10137–10141.
(8) Murphy, R. J.; Muthukumar, M. *J. Chem. Phys.* **2007**, *126*, 071101.
(9) Oukhaled, G.; Bacri, L.; Mathé, J.; Pelta, J.; Auvray, L. *Eur. Phys. Lett.* **2008**, *82*, 48003.
(10) Brun, L.; Pastoriza-Gallego, M.; Oukhaled, G.; Mathé, J.; Bacri, L.; Auvray, L.; Pelta, J. *Phys. Rev. Lett.* **2008**, *100*, 158302.
(11) Gibrat, G.; Pastoriza-Gallego, M.; Thiebot, B.; Breton, M.; Auvray, L.; Pelta, J. *J. Phys. Chem. B* **2008**, *112*, 14687–14691.
(12) Kasianowicz, J. J.; Brandin, E.; Branton, D.; Deamer, D. W. *Proc. Natl. Acad. Sci. U.S.A.* **1996**, *93*, 13770–13773.
(13) Akeson, M.; Branton, D.; Kasianowicz, J. J.; Brandin, E.; Deamer, D. W. *Biophys. J.* **1999**, *77*, 3227–3233.
(14) Meller, A.; Branton, D. *Electrophoresis* **2002**, *23*, 2583–2591.
(15) Oukhaled, G.; Mathé, J.; Biance, A.; Bacri, L.; Betton, J.; Lairez, D.; Pelta, J.; Auvray, L. *Phys. Rev. Lett.* **2007**, *98*, 158101.
(16) Stefureac, R.; Waldner, L.; Howard, P.; Lee, J. *Small* **2008**, *4*, 59–63.
(17) Pastoriza-Gallego, M.; Oukhaled, G.; Mathé, J.; Thiebot, B.; Betton, J.; Auvray, L.; Pelta, J. *FEBS Lett.* **2007**, *581*, 3371–3376.
(18) Saleh, O. A.; Sohn, L. L. *Rev. Sci. Instrum.* **2001**, *72*, 4449–4451.
(19) Saleh, O. A.; Sohn, L. L. *Nano Lett.* **2003**, *3*, 37–38.
(20) Picollet-D'Hahan, N.; Amatore, C.; Arbaul, S.; Thouin, L.; Biance, A.-L.; Oukhaled, G.; Auvray, L.; Weber, J.; Minc, N.; Viovy, J.-L. In *Nanoscience*; Springer: New York, 2009.
(21) Sun, Li.; Crooks, R. M. *J. Am. Chem. Soc.* **2000**, *122*, 12340–12345.
(22) Li, J.; Stein, D.; McMullan, C.; Branton, D.; Aziz, M. J.; Golovchenko, J. A. *Nature* **2001**, *412*, 166–169.
(23) Storm, A. J.; Chen, J. H.; Ling, X. S.; Zandbergen, H. W.; Dekker, C. *Nat. Mater.* **2003**, *2*, 537–540.
(24) Heins, A. H.; Siwy, Z. S.; Baker, L. A.; Martin, C. R. *Nano Lett.* **2005**, *5*, 1824–1829.
(25) Steinbock, L. J.; Otto, O.; Chimerel, C.; Gornall, J.; Keyser, U. F. *Nano Lett.* **2010**, *10*, 2493–2497.
(26) Steinbock, L. J.; Stober, G.; Keyser, U. F. *Biosens. Bioelectron.* **2009**, *24*, 2423–2427.
(27) Ito, T.; Sun, L.; Crooks, R. M. *Anal. Chem.* **2003**, *75*, 2399–2406.
(28) Ito, T.; Sun, Li.; Henriquez, R. R.; Crooks, R. M. *Acc. Chem. Res.* **2004**, *37*, 937–945.
(29) Henriquez, R. R.; Ito, T.; Sun, Li.; Crooks, R. M. *Analyst.* **2004**, *129*, 478–482.
(30) Petrossian, L.; Wilk, S. J.; Joshi, P.; Goodnick, S. M.; Thornton, T. J. *J. Phys. (Paris)* **2008**, *109*, 012028.
(31) Schiedt, B.; Auvray, L.; Bacri, L.; Biance, A.-L.; Madouri, A.; Bourhis, E.; Patriarche, G.; Pelta, J.; Jede, R.; Gierak, J. *Mater. Res. Soc. Symp. Proc.* **2009**, 1191.
(32) Stoeber, W.; Fink, A.; Bohn, E. *J. Colloid Interface Sci.* **1968**, *26*, 62.
(33) Castaing, J.-C. Unpublished Ph.D. Thesis, Pierre and Marie Curie University, 1996
(34) Rayleigh, L *Philos. Mag.* **1892**, *34*, 481.
(35) Henrickson, S. E.; Misakian, M.; Roberston, B.; Kasianowicz, J. J. *Phys. Rev. Lett.* **2000**, *85*, 3057.
(36) Costa, C. A. R.; Leite, C. A. P.; Galembeck, F. *Langmuir* **2006**, *22*, 7159–7166.
(37) Pastoriza-Gallego, M.; Rabah, L.; Gibrat, G.; Thiebot, B.; van der Goot, F. G.; Auvray, L.; Betton, J. M.; Pelta, J. *J. Am. Chem. Soc.* **2011**, 10.1021/ja1073245.

(38) Oukhaled, A.; Cressiot, B.; Bacri, L.; Pastoriza-Gallego, M.; Betton, J.-M.; Bourhis, E.; Jede, R.; Pelta, J.; Gierak, J.; Auvray, L. *ACS Nano* **2011**, in revision.
(39) Reguera, D.; G. Scmid, G.; Burada, P. S.; Rubi, J. M.; Reimann, P.; P. Hänggi, P. *Phys. Rev. Lett.* **2000**, *96*, 130603.
(40) Kantor, Y.; Kardar, M. *Phys. Rev. E* **2004**, *69*, 021806.
(41) Hänggi, P.; Talkner, P.; Borkovec, M. *Rev. Mod. Phys.* **1990**, *62*, 251.